Instrument Science Report WFC3 2010-10

WFC3 UVIS Full Well Depths, and Linearity Near and Beyond Saturation

R. L. Gilliland, A. Rajan, & S. Deustua

gillil@stsci.edu

October 2010

Abstract

Maps of the full well depth at which saturation sets in are provided for the two UVIS CCDs on WFC3. The full well depths show about 10% variation over each CCD ranging from 63-71K on UVIS1 and 67-72K on UVIS2. The standard gain of ∼1.6 e-/DN results in saturation safely being on the CCD rather than in the ADC, and linearity for photometry holds to levels better than 1% generally for UVIS2 to well beyond saturation simply from summation over pixels that have been bled into as a result of over-saturation. For UVIS1 the simple approach to saturated point source photometry shows deviations from linearity up to ∼15% for oversaturations exceeding 20, but the deviations are easily calibrated enabling linearity to be retained to near 1% even for stars over-saturated by 7 magnitudes.

1. Introduction

The spatial variation of CCD full well depths will be quantified for both UVIS CCDs. This calibration is in principle as simple as evaluating the maximum data value reached in a large number of saturated stars over the field of view, recording this as local values of the full well depth, then smoothing as appropriate. This would be true if the standard

definition of saturation held, namely that no more charge could be added to pixels after reaching this level. In practice this strict definition does not hold – as a pixel experiences successively greater degrees of over-saturation the recorded count level continues to creep upwards in a logarithmic sense. After taking the latter effect into account it is possible to derive the full well depths quite easily from simple analysis of hundreds of randomly positioned lightly saturated stars.

Experience from WFPC2 (Gilliland 1994), and especially STIS (Gilliland, Goudfrooij, and Kimble 1999) and ACS (Gilliland 2004) showed to some surprise that with use of a gain that samples the full well depth, the photometric response remains linear not only up to saturation, but also to well beyond saturation. Science applications of saturated star photometry or spectroscopy are quite common, sometimes with saturation being exceeded intentionally as a means of reaching high signal-to-noise limits, sometimes as a means of recovering photometry serendipitously on sources that were saturated by chance. Since long exposures ($\gtrsim$ 350 s) can be obtained very efficiently with WFC3, while shorter exposures often incur a large overhead to absorb ensuing buffer dumps, it is often the case that imaging data will have many saturated sources. An ability to recover excellent photometry for these saturated sources extends the value of much archival data.

The WFC3 CCDs have proven to be slightly more "interesting" than those for STIS or ACS in that one of the two chips (UVIS1) exhibits significant deviations from linearity in saturated targets, even after inclusion of counts from all pixels containing spilled charge. Fortunately, a relatively simple correction procedure allows recovery of linear photometry to large multiplicative values beyond the onset of saturation.

2. Observations

With a goal of testing for linearity to less than 1% we rely on having access to data that allows simple differential comparisons between high S/N unsaturated stars in short exposures and those same stars now saturated, in the long exposures. Rajan, Deustua, and Gilliland (2010) have analyzed data relevant to linearity of the WFC3 CCDs in all regimes below saturation. For this ISR we have located 4 WFC3 calibration and science programs with archival data providing back-to-back exposures on rich star fields with exposure time ratios ranging from 10 to 60.

In all cases, assessment of the short and long image pairs were made checking to verify that the exposures maintained pointing to less than 0.05 pixels and that the change of sky level across the two exposures was sufficiently close to the exposure time ratio that any

errors introduced by not carrying a correction for sky would remain small compared to Poisson fluctuations on the star counts.

Data from the following programs have proven to be most useful:

1. GO-11688. The GO observed the dense open cluster NGC 6819 to acquire first epoch data in support of proper motion observations. For these calibration purposes pairs of 10s and 600s exposures in both F606W and F814W were utilized. These data are ideal for assessing linearity beyond saturation since the short exposures contain many stars at unsaturated levels that in the long exposures reach into the strongly saturated regime. All data were acquired between 9-22 October 2009. After checking that mutual pointing and sky changes remained within acceptable bounds, 6 of the 8 visits were retained for analysis here. The 12 exposures used are listed in Table 1.

2. CAL-11452. This program observed 47 Tuc during SMOV for the purpose of measuring low-frequency flat fields generally. Short exposures of 35 s were taken in F438W, F606W and F814W followed by long exposures of 350 s at the central dither positions. We use only these three pairs of data, and verified that common pointing and expected sky changes implied that no corrections for these terms would be needed in comparing simple aperture photometry. The short exposures had been obtained to: (a) allow determination of field dependent PSFs, and (b) determine filter-to-filter offsets. These data were taken 18 July 2009. Table 1 details the exposures used.

3. CAL-11924. This program observes the dense open cluster NGC 6791 to assess changes in charge transfer efficiency (CTE) for WFC3. Six pairs of 30 and 360 s exposures in F606W are available for use here. The observations used come from Visit 1 on 2 October 2009 and Visit 2 on 25 March 2010.

4. CAL-11925. This program observes NGC 1850 for the express purpose of assessing UVIS detector linearity. We use only two sets of 10 and 500 s exposures in F467M taken back-to-back. These data were taken on 20 October 2009.

Most of the separate image pairs within programs involved large scale dithers at the full detector scale, thus providing fresh sets of stars at unique positions on the CCDs. These data suffice to provide a robust basis for defining the spatial dependence of full well depths, testing for linearity near and beyond saturation, and for developing and assessing the adequacy of any calibrations required to regain linearity as will be needed for UVIS1.

3. Full Well Depths

As noted previously in similar STIS and ACS calibrations, the number of recorded electrons in pixels that have been exposed beyond saturation do not remain at a strictly constant level, but rather continue to slowly increase with the degree of over-saturation. In order to derive the spatial distribution of full well depth, which we take to be the point at which charge spilling starts to occur from the central pixel, it is necessary to first calibrate the "pile-up" effect which relates count levels reached in saturated images to the degree of over-saturation. Then, with this in hand it is possible to use stars with arbitrary over-saturation levels and predict what the count level was at the onset of saturation.

Performing photometry on severely saturated images is best done in the direct **flt** images (although in principle it still works in the drizzled images) using simple aperture photometry, and requires a special approach to aperture definition. For the purposes here the extraction aperture is always defined to be: (a) a core region consisting of the central 37 pixels – essentially adopting a radius of ∼3.5 pixels, and augmented by (b) any additional pixels that are needed to encompass all pixels that have been bled into with the long exposure. The latter is accomplished simply by stepping outwards along rows and columns and recording all contiguous pixels that remain above a specified threshold which we have adopted as 12,000 e-. Then a buffer of 1 pixel in all directions is added to account for possible charge diffusion. The results are insensitive to details, e.g. adopting a core aperture of 5 pixels radius and augmenting with a 2 pixel halo buffer has been tried and makes no discernible difference in the results.

The above approach to aperture definition results in oddly shaped apertures that trace the flux for strongly saturated stars. This is necessary as opposed to simply adopting a circular aperture large enough to capture all of the rows that have been bled into along the saturation columns. In extreme cases we perform photometry on stars that have bled to more than 1,000 pixels edge-to-edge that in this approach results in apertures with about 3,000 pixels, a circular aperture needed to capture all the bleeding would encompass some 750,000 pixels and in doing so would include many other stars. In this calibration it is critical that the aperture adopted for the long exposure also be applied to the short exposure so that the flux from any faint background sources and sky enters properly. Figure 1 illustrates this approach to aperture selection.

With appropriate data identified as in Table 1, and an approach to defining apertures as shown in Figure 1, the next step is to identify a set of stars to use. Some stars are strongly saturated in even the short exposures, but since those typically number only a handful per data set a pass by hand was made over all the images to record such cases as they are not easily amenable to automated searches. The primary search technique

Fig. 1.— Illustrates aperture definition for saturated stars by showing 512x512 regions of a pair of CAL-11452 exposures on 47 Tuc and associated apertures adopted. The upper left quadrant of the figure shows data from the 350s F606W exposure, the upper right shows the respective short 35s F606W data. Below each are the apertures adopted to capture all of the flux for saturated stars in the long exposure; the same apertures are used for the short exposure.

has been to identify all positions of local maxima (pixel brighter than neighbors at all 8 permutations of ± 1) in the short exposure, then perform a series of logical tests based on this value, the sum of neighboring pixels, and the data value in the long exposure to select stars which will be at desired levels of over-saturation in the complementary long exposure. The logic includes enough tests to very effectively avoid identifying cosmic rays as sources. We then tabulate a number of values associated with each star in both the short and long exposures: maximum values in short and long exposures within $\pm$ 1 of star center, sum of counts in aperture for both long and short, and the number of pixels that are above about 90% of the minimal full well depth for the respective CCDs (this 90% limit is taken as 60,000 e- for UVIS1, 63,000 e- for UVIS2). This latter value is a good measure of how many pixels have reached saturation for each star.

Figure 2 shows the distribution of maximum data value associated with saturated stars plotted against the number of saturated pixels for both UVIS CCDs. These results use all of the exposures detailed in Table 1. The value on the y-axis is normalized to the local full well depth, which is only defined after following what is an iterative procedure. The 'pile-up' of counts that depends upon the degree of over-saturation is clearly visible in Figure 2, and can be represented as a simple linear fit to the number of saturated pixels. The level of over-saturation may be defined as the number of counts in the aperture sum divided by the number of counts that exist when the central pixel for a star first reaches full well depth. With this definition an over-saturation of X results in about 4X saturated pixels. Figure 2 thus shows that by the time a star is over-saturated by a factor of 250 (6 magnitudes beyond saturation), the pixel count levels have crept up to about 33% above the nominal full well depth.

An interesting side issue to check is whether saturation at the nominal gain of 1.6 e-/DN will always occur on-chip, or whether the 'pile-up' effect can lead to saturation being limited by the 16 bit ADC. The bleeding extent along columns extends to roughly the number of saturated pixels divided by six. Thus a star centered on a CCD can produce a maximum of about 6,000 saturated pixels before having bled off the edge in which case photometry cannot be recovered in any case. The linear fits in Figure 2 show a slope of 0.1156, thus 6,000 pixels corresponds to a 'pile-up' of 1.44 times the nominal full well depth. As will be shown, the maximum full well depth reached on either CCD is about 72,000 e-. The maximum data value that can be reached for a star that does not bleed off the edge is thus 103,700 e-, which is just slightly smaller than the nominal value of 1.6 e- $\times$ 2^{16} = 105,000 e-. Saturation should occur on-chip in all cases that are not so over-saturated that they bleed off-chip anyway.

With knowledge of the 'pile-up' relation shown in Figure 2 it should now be a simple matter for each star to note the number of saturated pixels, then divide the associated maximum value recorded for that star by 1.0 + 0.1156$\times$log(number of saturated pixels) to arrive at the full well depth at the location of each star. A complication should be noted about the distribution of stars in Figure 2: for UVIS2 and UVIS1 respectively, we have included only stars from regions of the CCDs for which the ratio of counts in the long exposure divided by the counts in the short exposure remain within 2% of perfect linearity for stars at $\times$20-200 over-saturation in the long exposures. For UVIS2 such linearity holds for essentially the full CCD while for UVIS1 such linearity holds for only about 10% of the total area, with large areas of the CCD reaching deviations of 10-20% from linearity as just defined. Figure 3 is the same as Figure 2, but now showing just those stars pulled from regions on the CCDs for which the deviation from linearity falls within the 10-20% range. Clearly there is a qualitative difference in the degree of charge pile-up between those

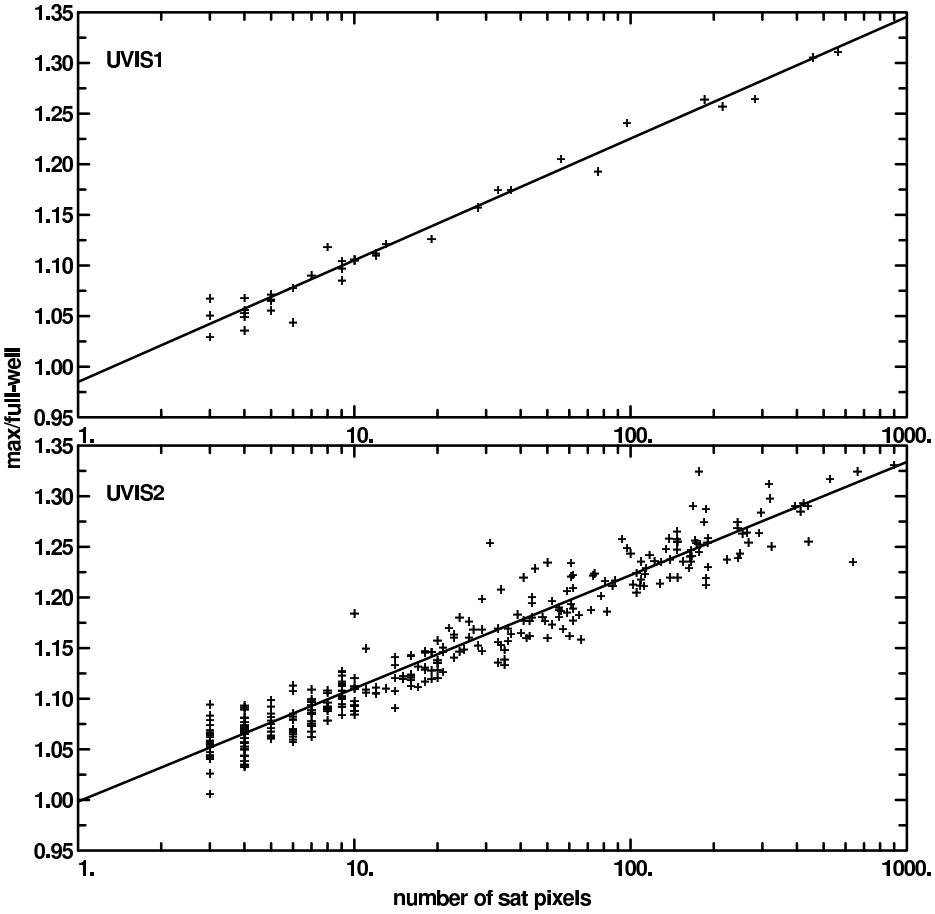

Fig. 2.— Panels (with UVIS1 at top, UVIS2 at bottom) show the ratio of maximum data value divided by local full well depth plotted against the number of saturated pixels as discussed in the text. Saturation is a slight misnomer for the behavior of strongly exposed CCD images, since in fact there is a 'pile-up' effect that leads to still logarithmically increasing count levels beyond the obvious point at which saturation as indicated by charge bleeding sets in. This figure is for stars that remain within 2% of linearity to well beyond saturation as discussed in the text.

regions of the CCD that provide linear response beyond saturation and those that do not. For now this difference is used merely as a tool to back out the level of full well depth for each star. Later this difference will provide a key hint and quantitative basis for calibrating the non-linearity that has been encountered.

For the regions of CCDs providing non-linear response we linearly interpolate in the slope of 0.1156 shown in Figure 2 for linear domains, and a slope of 0.03 for domains in which the ratio of long exposure counts to short falls 12% short of linearity. Figure 4 shows

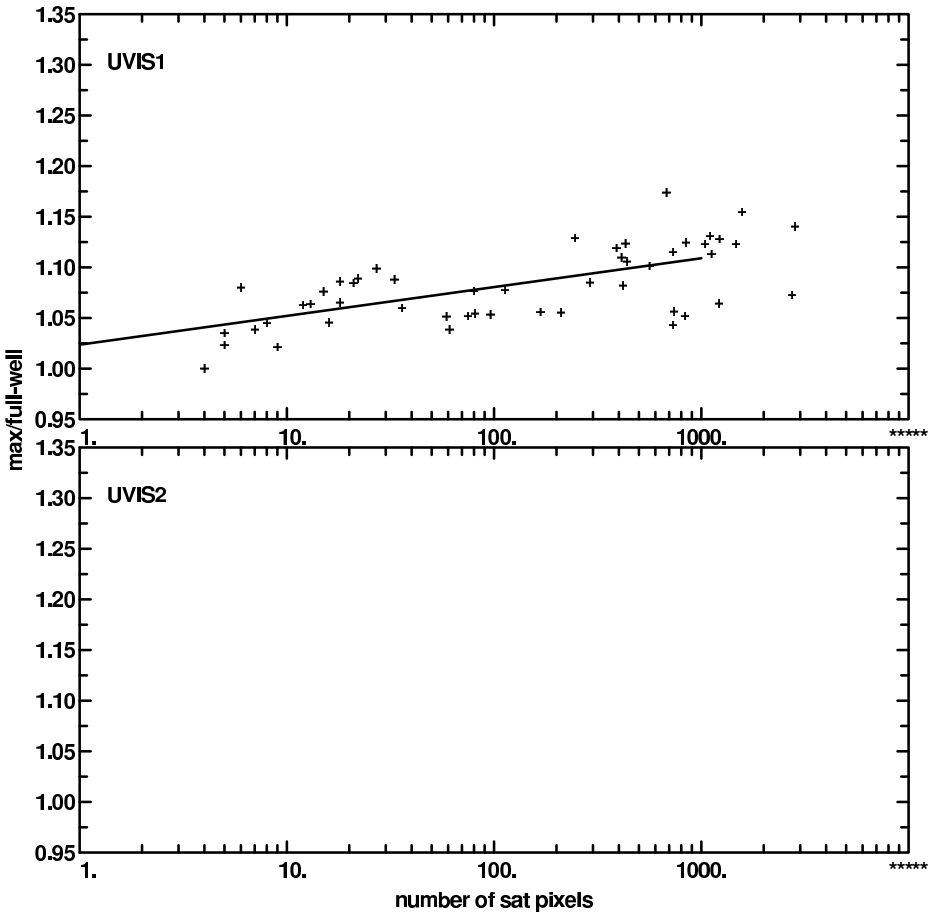

Fig. 3.— Same as Figure 2, but for just the regions on CCDs where a measure of deviation from linearity for strongly saturated stars exceeds 10%. Clearly where UVIS1 is non-linear beyond saturation the 'pile-up' effect shown so consistently for linear regions of both UVIS1 and UVIS2 in Figure 2, deviates strongly to less continued accumulation of charge. Note that no regions on UVIS2 reach the 10% nonlinearity threshold, thus leaving the lower panel unpopulated.

the corresponding map of which regions of the CCDs are at various levels of non-linear response.

Using stars having just 3 – 7 saturated pixels, and applying a correction for the 'pile-up' effect discussed above results in 313 stars with projected values of maximum data values where saturation just sets in, i.e., the local full well depth. These x, y distributions of local full well depth values are then smoothed with a Gaussian function with width of 400 pixels to arrive at the full well depth distribution shown in Figure 5. On average, 15 values contribute to each Gaussian weighted sum in this map. Dispersion in the full well

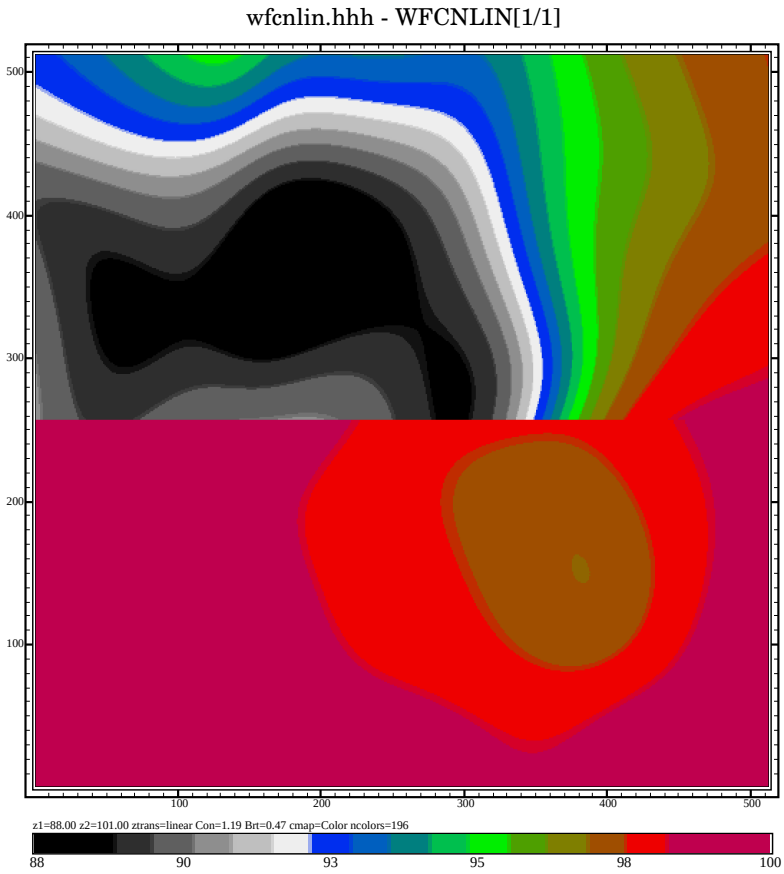

Fig. 4.— A distribution of deviations from linearity after smoothing local values by a Gaussian of width 400 pixels. The color table is such that the dominant area of UVIS2 (bottom) corresponds to 99% to 101%, or perfect linearity within nominal errors. On UVIS2 the most deviant area reaches under 98% for only a small area. For UVIS1 (top) the lowest values (black) are at 88% of perfect linearity and most of the area falls below 98% of linearity. See text for further explanation.

depths contributing to local sums averages less than 500 e-, while peak-to-peak variations in full well depth over the CCDs reaches several thousand – the deviations found are quite significant. The full well depth on UVIS1 ranges from 63300 e- to 71100 e-, while UVIS2 shows a slightly higher and less variable range of 66850 e- to 72500 e-.

These values for the full well depth are some 10% lower than the 75-80K e- quoted in the Instrument Handbook based on ground testing. The simplest explanation for this is that the ground testing results relied on either flat fields, or sources that were large compared to point sources. Either of these builds in expectation of a significant 'pile-up' effect that was

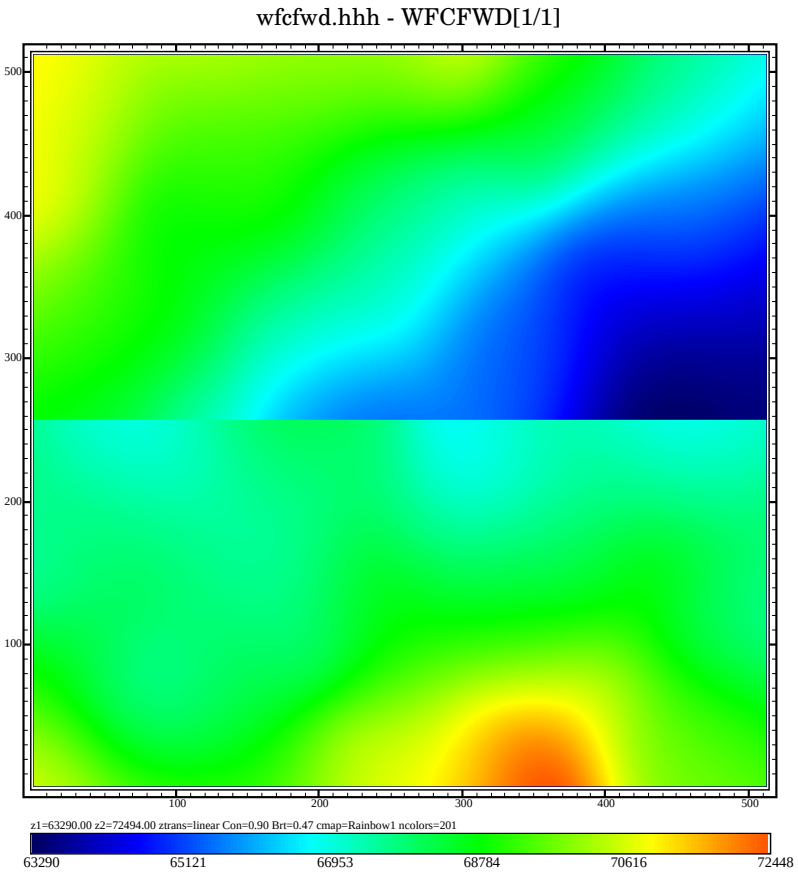

Fig. 5.— The distribution of full well depth for UVIS1 (top) and UVIS2 (bottom) taken to be the number of electrons at which charge spilling just starts to set in for point sources. Local values derived for 313 stars have been smoothed with a Gaussian of width 400 pixels to produce this map.

not then allowed for in assessing at what level the spatially non-linear saturation for point sources sets in.

Access to the numerical values of the full well depth will be needed to support the photometric corrections discussed in the next section (for Eq. 1). Fits files for these are named UVIS[1,2]wfc3_fwd.fits and may be found at: http://www.stsci.edu/hst/wfc3/analysis/full_well_depth.

4. Linearity Beyond Saturation

The extent to which accurate photometry can be extracted for point sources in which one or more pixels have exceeded the physical full well depth are explored here. The basic approach relies on assignment of apertures in long exposures as necessary to capture all of the flux, applying this same aperture to extract photometry in well-registered, back-to-back short and long exposures in the same filter, and then simply checking to see if the ratio of long to short counts is equal to the ratio of exposure times as expected for a linear response.

Figure 6 provides a summary of photometry near and beyond saturation for the Amp C quadrant of UVIS2 (left half of the chip) for which preliminary assessment as shown in Figure 4 suggested linearity is well preserved up to over-saturation levels of about 50, with only deviations of a few percent even well beyond this.

By contrast Figure 7 shows the same response on the Amp A quadrant of UVIS1 (left half of the chip). Already at over-saturation levels of a few there are noticeable deviations from linearity, with nearly 20% losses being accumulated.

We are using exposures for which neither CR-SPLITs nor small dithers are available, and therefore robust elimination of cosmic rays is not possible. We do, however, provide arguments here showing that cosmic rays, which will certainly be present within some of the apertures analyzed are not a serious limitation for establishing linearity near and beyond saturation. A typical value for number of pixels impacted by cosmic rays is 2% per 1,000 second exposure. The actual number of events will be about a factor of 5 lower than this, with 5 pixels per event. Therefore in a 600 s exposure, the longest used here, and allowing an added 100 s for readout (this argument is only being worked up to factor of two accuracy) there would be a total of some 45,000 events over the full 16 Mpixels, or one event per 350 pixels. For a typical short exposure time in which the 100 s readout time dominates there would be one event per 2500 pixels. For even an over-saturated by 200 star the number of pixels in its aperture will be only about 1,000. Therefore the short exposure for such a star would typically not have a single cosmic ray hit in the aperture, while the long exposure would have on average about 3 events. The number of counts from this star will be about 7.6 $\times 10^7$ e- in the 600 s exposure and 1.26 $\times 10^6$ e- in the short exposure. Each cosmic ray event averages some 1,000 e-. Common cosmic ray events would change the ratio of long to short count ratios by less than one part in a thousand, and will cancel out to first order anyway with more appearing in the long than short exposures. Statistically cosmic rays seem very unimportant. This rough analysis indicates that the impact of cosmic rays falls short by nearly 3 orders of magnitude in explaining deviations evident in Figure 7, and would not in any case lead to spatially dependent effects seen in Figure 4. For much fainter stars, e.g. those appearing with "over-saturation" levels well

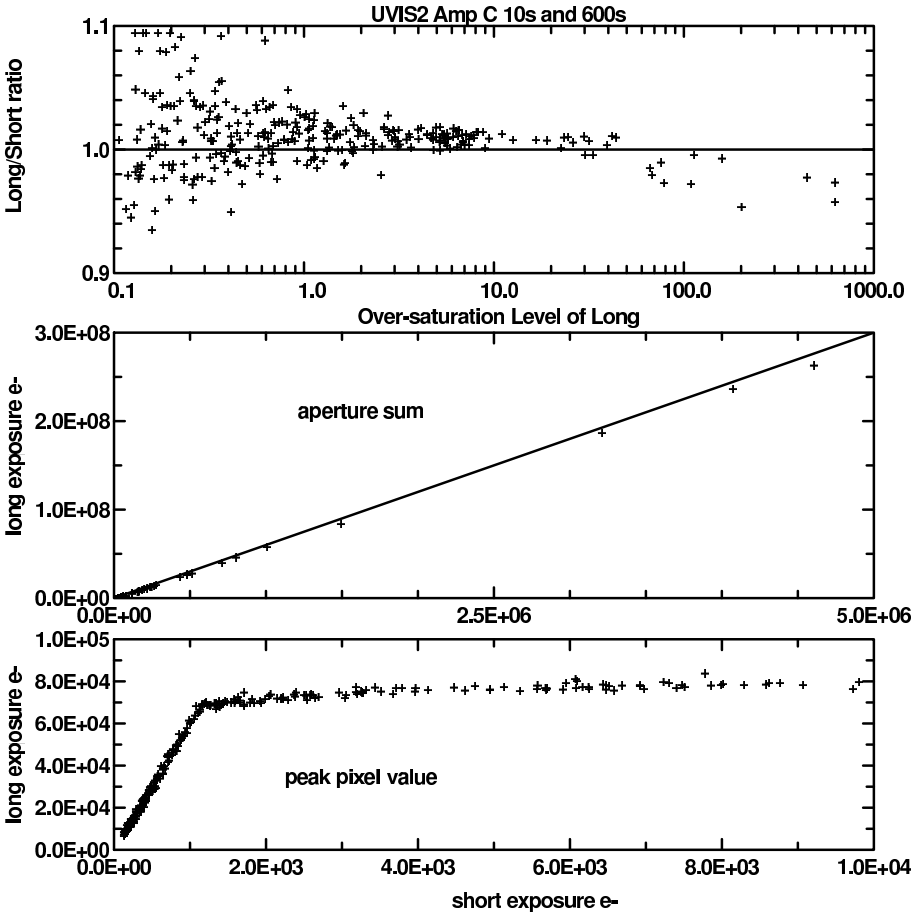

Fig. 6.— Analysis of linearity beyond saturation for Amp C on UVIS2. The upper panel shows the ratio of counts in the long exposure divided by the counts in the short exposure multiplied by the relative exposure time; linearity would thus result in a value of unity. The x-axis shows the multiplicative degree by which a star is over-saturated in the long exposure. The middle panel plots long exposure aperture sums versus short exposure aperture sums. The lower panel shows the peak data value in the long exposure versus that from the short exposure – this has the slope of relative exposure time up to the point at which saturation starts to set in near 68,000 e-. Amp C appears linear for over-saturations up to $\sim \times 50$, with deviations up to 2-5% at much higher exposure levels.

under unity even in the long exposure, a cosmic ray hit in one or the other exposure can significantly perturb the ratio, but with only 37 pixels carried for the apertures, even the long exposure should have a cosmic ray hitting only 1 in every 10 stars, and when it does at an over-saturation of 0.2 would result in perturbing the ratio upwards by about 1%. Cosmic rays are irrelevant to considerations beyond saturation, and should be only a minor

contaminant in explaining why the ratios in the upper panel of Figures 6 and 7 are above unity for the lowest count levels.

We have verified that the results in this ISR are not sensitive to deviations in small apertures that may sometimes result from telescope "breathing".

We are also not applying corrections for sky levels between the long and short exposures, assuming and checking that such is adequately true, that the ratio of sky levels will also follow the ratio of exposure times and therefore not contribute to errors regarding linearity or lack thereof. We have evaluated global mean sky values for each of the long and short image pairs used for analyses in this section. The global means use all pixels that fall within 4 σ of the nominal sky values in both the short and long exposures. The sky value in the short exposures does closely track the values in the long exposure divided by the exposure time ratio. Deviation of short exposure sky to long divided by the relative exposure time averages -0.04 $\pm$ 0.10 e- (sense scaled long - short) on an average sky of 0.4 e- per pixel in the short exposures. Errors on sky per frame are perhaps 1 e- (long) and 0.1 e- (short). For an over-saturated by 200 star with 1,000 pixels in the aperture, errors from not having corrected for the sky might therefore be 1,000 e- for the long exposure (out of 7.6 $\times 10^7$ e- on the star), and 100 e- for the short exposure (out of 1.26 $\times 10^6$ e-). Thus errors resulting from ignoring sky corrections are (a) well under one part per thousand, and (b) well under the Poisson fluctuations from the target. Similarly, consider a case in which the long exposure reaches 0.2 of saturation, or about 76,000 e- within 37 pixels – the error from sky can be 37 e-, less than a part per thousand and a factor of 8 below the Poisson limit on counts. In the short exposure there would be 1270 e- in the star sum with an error of 4 e- from sky, for a potential error of 0.3% compared to a 2.8% Poisson uncertainty for the same star. Uncompensated sky levels are irrelevant to considerations beyond saturation, and should be only a minor contaminant in explaining why the ratios in the upper panel of Figures 6 and 7 are above unity for the lowest could levels.

We now provide an effective calibration of the loss of linearity and document how to obtain excellent photometry on point sources well beyond the saturation limit. It was noted associated with Figures 2 and 3 that there is a qualitatively different response for the 'pile-up' effect within regions of the CCDs that show linear response and those that do not. In particular there is much less 'pile-up' of charge for stars that show strong deviations (in a negative sense) from linearity. A tested hypothesis was that the deficit in 'pile-up' corresponded to the same deficit in overall counts summed over an aperture that includes all the pixels that have been bled into. If this were true, then a simple correction procedure would be to use the linear relations in Figure 2 to project what the maximum data values should be, subtract from that the observed maximum value for a saturated star

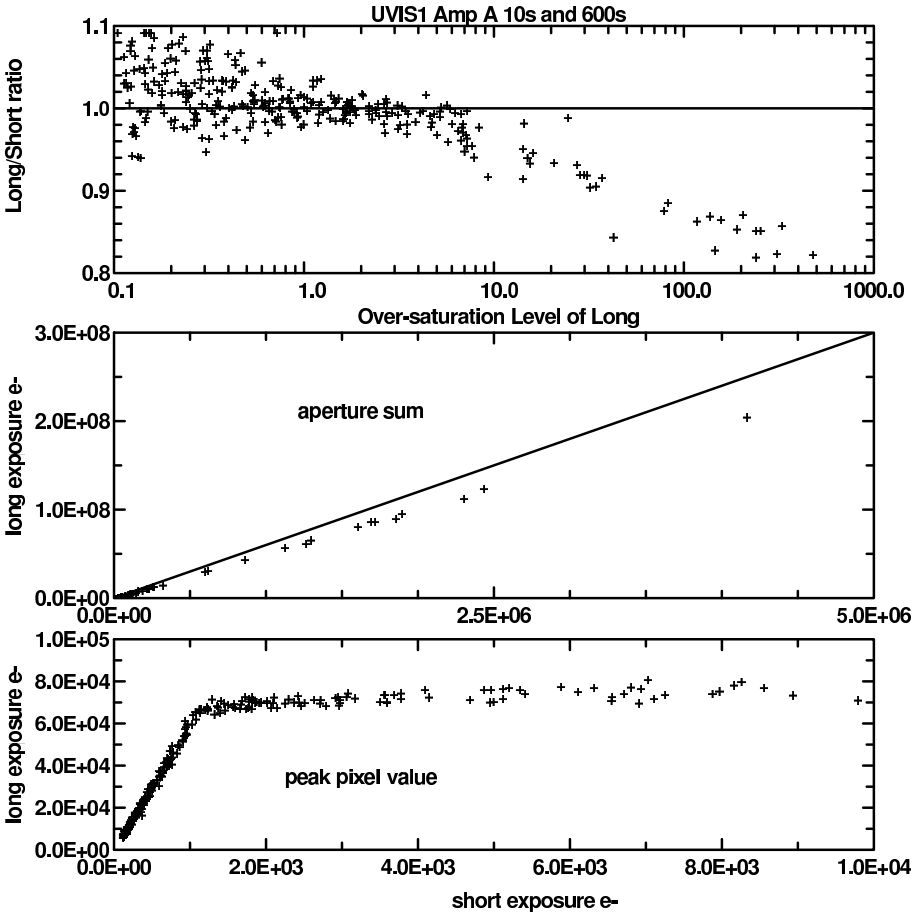

Fig. 7.— Same as Figure 6, but for Amp A of UVIS1. Note the expanded scale, however, in the upper panel. The deviations from linearity beyond saturation are much more acute for Amp A.

and multiply this difference by the number of saturated pixels to obtain a correction factor. This hypothesis survived a simple test by hand on a couple of highly non-linear stars, and has in fact resulted in a very effective prescription for the restoration of WFC3 UVIS data to linearity independent of degree of over-saturation.

The corrected photometric counts, CTS_c, follow from the observed aperture sum counts, CTS_o, as:

$$FWD_P = FWD * (afwd_i + bfwd_i * \log(N_{sat})) \quad (1)$$

$$CTS_c = CTS_o + N_{sat} * (FWD_P - data_{max}) \quad (2)$$

where N_{sat} are the number of pixels exceeding a level taken as 90% of saturation in the stellar image to be corrected, $data_{max}$ is the maximum data value in an **flt.fits** image within ±1 of the nominal stellar image center, FWD is the full well depth in e- at the position of the star evaluated from the data array for full well depth (see end of §3), FWD_P is the projected full well depth capturing the 'pile-up' effect as shown in Figure 2 for well behaved parts of the chips, $afwd_i$ and $bfwd_i$ are the linear coefficients that have been optimized for UVIS1 and UVIS2 respectively to return optimally corrected photometry. The correction factor in Eq. (2) is restricted to be positive, or set to zero. The linear coefficients $awfd_i$ are 0.905 and 0.880 for UVIS1 and UVIS2 respectively, while the slope terms $bwfd_i$ are 0.1415 and 0.163. These coefficients were developed using the data from GO-11688 with 600, 10 second image pairs in both F606W and F814W, and were verified by equally successful application to the 360, 30 second image pairs in F606W from CAL-11924.

Figure 8 shows the full set of original data value ratios for UVIS1 (Amps A and B), plus the same set of data after applying the simple additive correction outlined above. Note that before correction, at high levels of oversaturation the UVIS1 data show widely varying deviations from linearity. The simple corrective procedure successfully restores count levels for stars needing large corrections, and importantly at the same time automatically does not apply significant corrections where none are needed.

Figures 9 and 10 show the overall improvements provided for UVIS1 and UVIS2. For UVIS1 Figure 8 showed the individual photometry values before and after correction with Eqs (1) and (2), while Figure 9 shows the same but now after averaging over equally spaced intervals in over-saturation. For all 10 bins over both CCDs beyond an over-saturation of 5 the largest deviations in the mean are under 1%, and the standard deviations within bins for the corrected data are $\leq 1.5\%$ in nearly all cases.

5. Linearity Below Saturation

Arguably the most interesting feature of Figures 8 - 10 is the deviation above unity at low count levels in the normalized long to short ratios. Here the behavior of counts

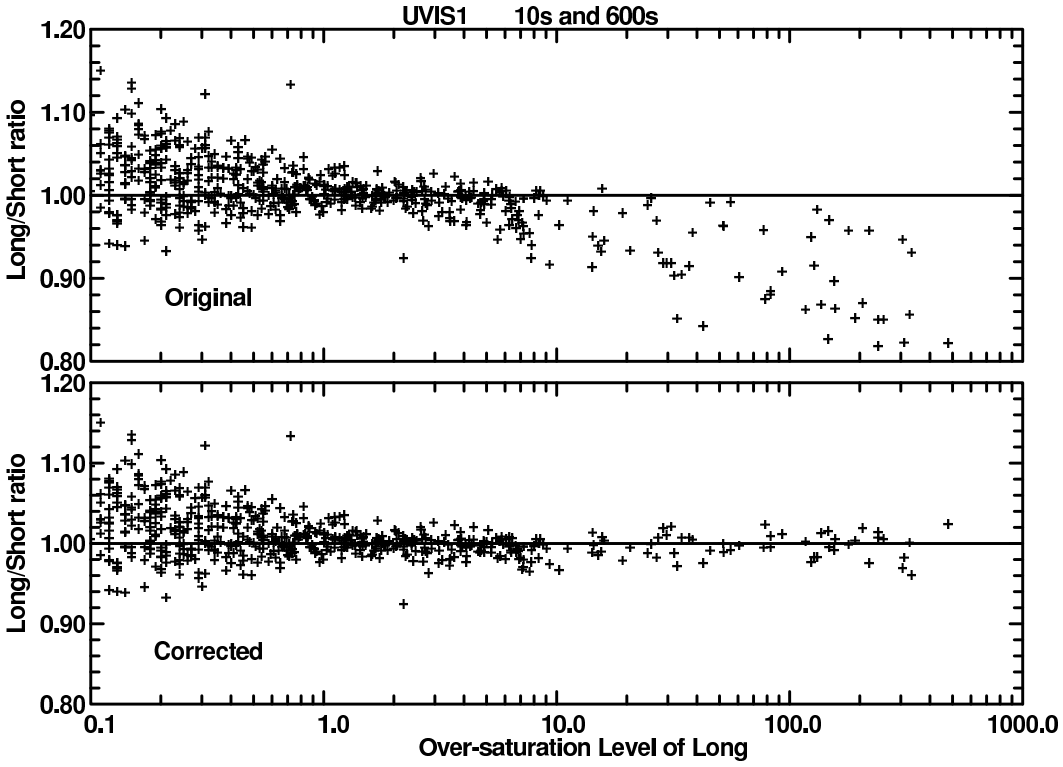

Fig. 8.— Upper panel shows data of upper panel of Figure 7 for Amp A, plus similar for Amp B. The lower panel shows the same data after applying the corrections given in detail by Equations (1) - (2). Not only is the mean level appropriately restored independent of degree of oversaturation, but the star-to-star scatter is much reduced.

contributing to the lowest "over-saturation" bin in Figures 9 and 10 is further explored. The mean "over-saturation" level of stars in this first bin is 0.16. With a global mean full well depth of 68,055 e-, and mean ratio of central pixel value to 37-pixel aperture sum of 0.17 for these data this translates to a mean count level of 64,050 e- for the long exposures and 1,067 e- for the same stars in the short exposures. The S/N of the short exposure stars including readout noise and Poisson errors translates to an expected 0.036 error per star, which is close to, but somewhat smaller than the empirical scatter as seen in these figures.

The first bin for UVIS1 is at a mean of 1.033, with standard deviation of 0.043, and a standard error on the mean of 0.004 e-. For UVIS2 the mean is 1.018, standard deviation of 0.048 and standard error of 0.005 e-. The mean offset of the first bin is 8 and 4 σ for UVIS1 and UVIS2 respectively.

We argued in the previous section that neither cosmic rays, nor uncompensated sky levels could contribute significantly to the greater than unity ratio of long to short exposure

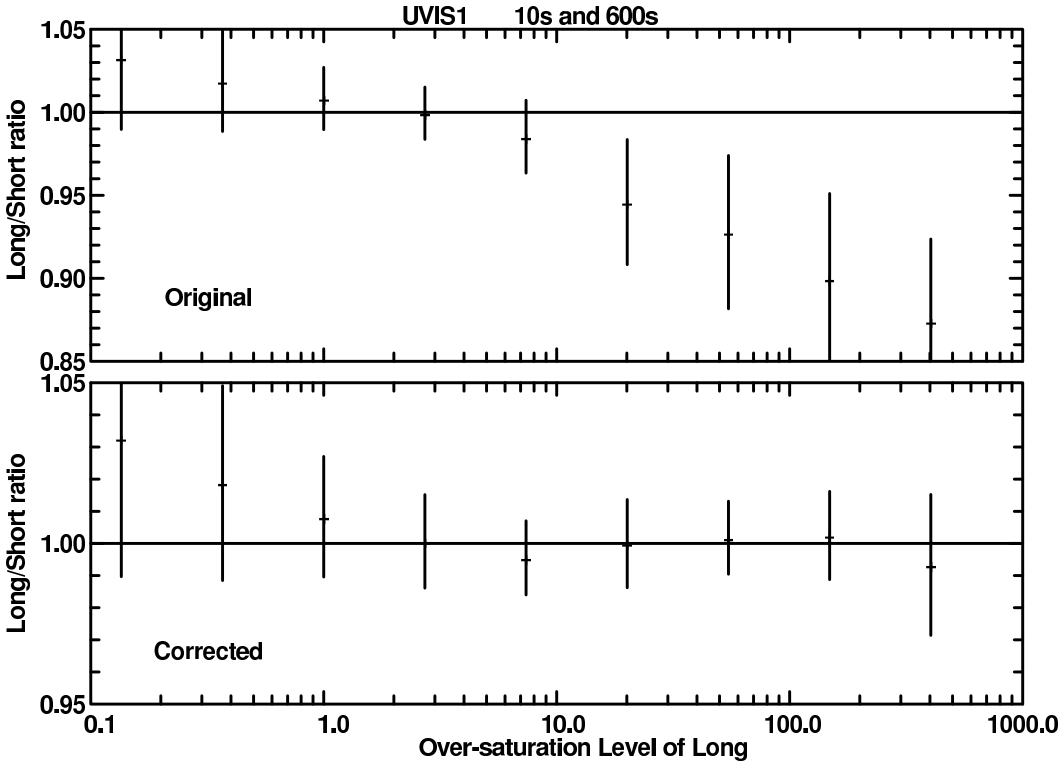

Fig. 9.— Upper panel shows mean ratios of the long to short exposure sums normalized by the exposure time ratio in natural log intervals of the over-saturation level. The standard deviation within bins is shown as the vertical lines at each point. The lower panel shows the same after individual stars were corrected using Eqs (1) and (2).

counts. Since this same effect has been seen consistently in a large number of short and long image pairs it does not seem likely to result from breathing having led to a broader PSF in the short compared to long exposure. Likewise, small errors in the PSF can be induced from jitter caused by one of the two UVIS shutters (Sabbi 2009), but for these 10 s exposures this too is expected to fall far short of creating a sufficient deficit in the short exposure counts to explain the effects seen in Figures 8 - 10.

A potentially viable hypothesis is to invoke a well-known non-linearity of limited Charge Transfer Efficiency which affects low intensity exposures, and those with low sky more than well exposed stellar images or those with significant sky background. A characteristic of CTE losses with ACS is a strong dependence of lost flux on the number of parallel shifts (distance in y from readout amplifier), and this will be the expected signature with WFC3 when significant losses eventually result from radiation damage on orbit. Figure 11 shows the deviations in stars for the lowest bin for Amp C of UVIS2.

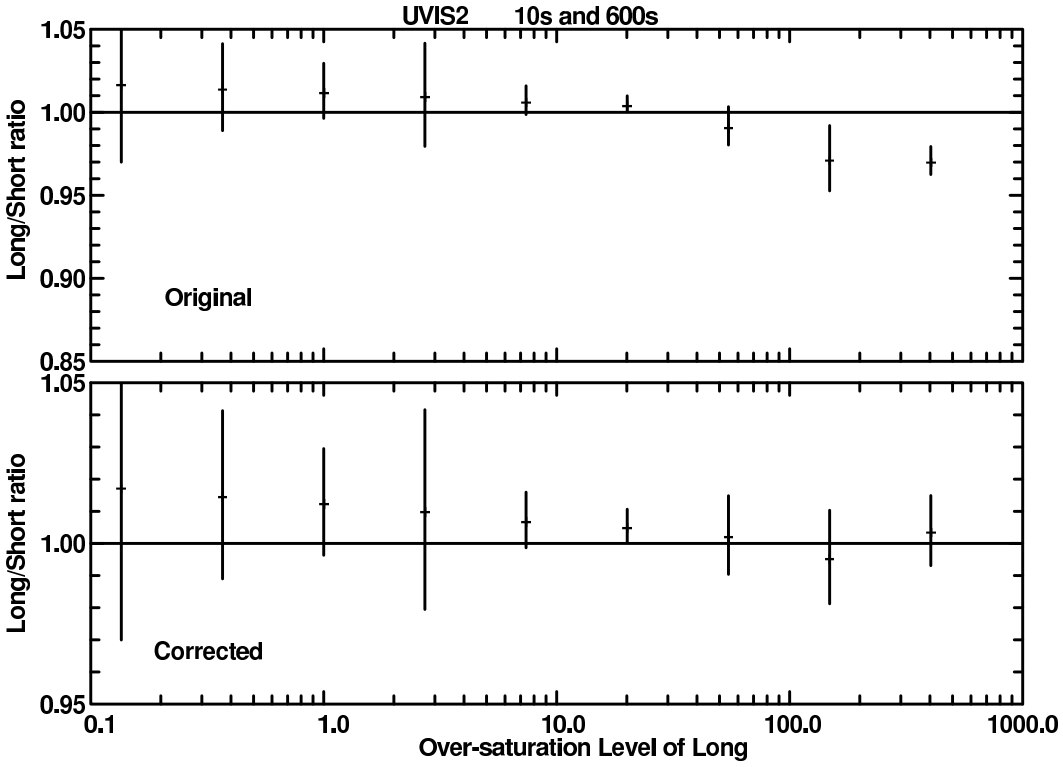

Fig. 10.— Same as Figure 9 but for UVIS2.

There is a distinct trend of greater loss with distance in y away from the readout amplifier. All four amplifiers for WFC3 show similar effects, for Amps A and B the slope in y is negative (amplifiers at $y = 2048$) while Amps C and D both show positive slopes. The average slope in y over all 4 amplifiers is 2.4 $\times 10^{-5}$ per pixel for the relative deficiency in stars with summed counts of 1,067 e- (10 s) compared to those with 64,000 e- (600 s). For the full deficits in the lowest Figure 9 and 10 bins to follow from uncompensated parallel CTE loss the effect as of October 19, 2009 would need to be a loss of 3.3% for a star with 1,000 e- and a sky background of 0.4 e- for UVIS1 for 1,024 parallel transfers, and 1.8% for the same circumstances on UVIS2. Exploration of low exposure level non-linearity is more thoroughly explored in the ISR by Rajan, Deustua, and Gilliland (2010).

6. Summary

The full well depth has been derived as a function of position on UVIS1 and UVIS2. The definition of full well depth has been taken to be the maximum data value beyond which bleeding along columns does not occur. These values, which reflect the limiting

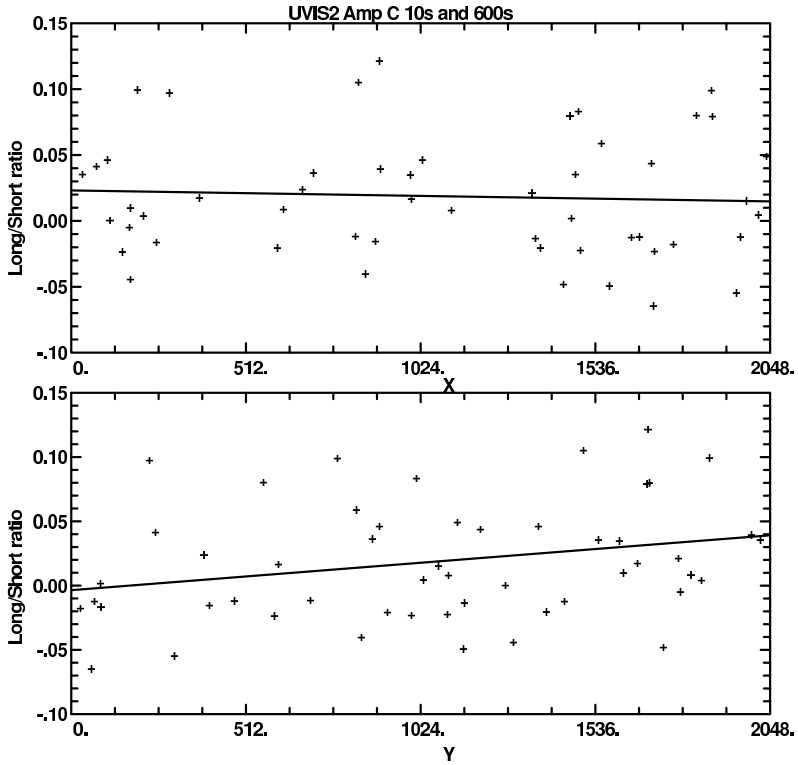

Fig. 11.— These panels show the deviations for the lowest intensity bin in Figure 8 for UVIS2, Amp C plotted against x (serial shifts) in the upper panel, and y (parallel shifts) in the lower panel. The correlation of deviations with y is significant, and suggestive of CTE losses.

exposure for which point sources will maintain spatial integrity, are some 10-15% lower than previously estimated values based on ground testing.

While the full well depth imposes a hard limit beyond which spatial nonlinearity begins, experience with STIS and ACS showed that photometric linearity nonetheless holds simply by summing the counts over all pixels including those containing bled charge, assuming the gain provides on-chip saturation (automatic for WFC3). For WFC3 the response is more "interesting" in that simply deriving aperture sums does not always provide linear response beyond saturation. It was noted during derivation of the full well depth that some regions of the CCDs (that are not automatically linear beyond saturation) show a maximum data value 'pile-up' effect that is much smaller than that in regions that do provide linear response. The difference between canonical maximum values, and those observed for saturated stars individually provided the motivation for a quite effective and very simple correction factor. This provides corrections to photometric response that will support photometry of WFC3/UVIS stellar sources that are up to 7 magnitudes beyond

saturation.

An interesting question is where the electrons have gone that represent the deviation from linearity beyond saturation. A simple hypothesis, that the charge has diffused to neighboring pixels, does not hold. Inspection of columns near saturated columns shows no evidence of significant charge diffusion. Use of arbitrarily larger apertures does not affect the final result. Another hypothesis might be that the electron–hole pairs recombine for the highly saturated pixels after being created. In this scenario a greater relative deficiency would be expected for the 600/10 second pairs (they have longer to recombine) used in Figs. 7–10, than if the available 360/30 second data were analyzed. Although not shown, the 360/30 second data show the same deficiencies in the direct data as in Fig. 7 and equally good corrections as in Fig. 8 – the charge loss does not seem to be a function of integration time. Perhaps the electrons are not created in the first place, e.g. the local quantum efficiency is lowered as saturated is exceeded. Or perhaps the electrons are lost via passing vertically through the CCD substrate and out of the well that is shuffled to the readout amplifier. The complicated spatial dependence of this non-linearity suggests the shift register and readout amplifier are absolved as causative agents.

I thank Luigi Bedin, the PI for GO-11688, for providing permission to use his still proprietary data in these calibrations. I thank Sylvia Baggett and John MacKenty for enlightenment on numerous WFC3 items, and Bruce Woodgate for discussion.

References

Gilliland, R. L. 1994, "Stellar Photometry Including Saturated Images: Results on M67 with WFPC2", ApJ, 435, L63-66.

Gilliland, R. L., Goudfrooij, P., and Kimble, R. A. 1999, "Linearity and High Signal-to-Noise Performance of the STIS CCD, PASP, 111, 1009-1020.

Gilliland, R. L. 2004, "ACS CCD Gains, Full Well Depths, and Linearity up to and Beyond Saturation", Instrument Science Report, ACS 2004-01,

Rajan, A., Deustua, S., and Gilliland, R. L. 2010 "WFC3 UVIS Linearity Near and Below Saturation", WFC3 ISR 2010-xx.

Sabbi, E. 2009, "WFC3 SMOV Program 11798: UVIS PSF Core Modulation," WFC3 ISR 2009-20. (Baltimore: STScI)

Table 1: Data Sets Used

Prop-ID	Date	Root-name	Filter	T_{exp} s
GO-11688	10/09/2009	ib2o01soq	F606W	10
GO-11688	10/09/2009	ib2o01spq	F606W	600
GO-11688	10/09/2009	ib2o02t2q	F606W	10
GO-11688	10/09/2009	ib2o02t3q	F606W	600
GO-11688	10/19/2009	ib2o03p8q	F606W	10
GO-11688	10/19/2009	ib2o03p9q	F606W	600
GO-11688	10/21/2009	ib2o05f4q	F814W	10
GO-11688	10/21/2009	ib2o05f5q	F814W	600
GO-11688	10/29/2009	ib2oa6utq	F814W	10
GO-11688	10/29/2009	ib2oa6ttq	F814W	600
GO-11688	10/30/2009	ib2o08vxq	F814W	10
GO-11688	10/30/2009	ib2o08vyq	F814W	600
CAL-11452	07/17/2009	iaby01kbq	F438W	35
CAL-11452	07/17/2009	iaby01kcq	F438W	350
CAL-11452	07/17/2009	iaby01kjq	F606W	35
CAL-11452	07/17/2009	iaby01khq	F606W	350
CAL-11452	07/17/2009	iaby01keq	F814W	35
CAL-11452	07/17/2009	iaby01kgq	F814W	350
CAL-11924	10/02/2009	ibc601gxq	F606W	30
CAL-11924	10/02/2009	ibc601h2q	F606W	360
CAL-11924	10/02/2009	ibc601gzq	F606W	30
CAL-11924	10/02/2009	ibc601h3q	F606W	360
CAL-11924	10/02/2009	ibc601h0q	F606W	30
CAL-11924	10/02/2009	ibc601h5q	F606W	360
CAL-11924	03/25/2010	ibc602v1q	F606W	30
CAL-11924	03/25/2010	ibc602v6q	F606W	360
CAL-11924	03/25/2010	ibc602v3q	F606W	30
CAL-11924	03/25/2010	ibc602v7q	F606W	360
CAL-11924	03/25/2010	ibc602v4q	F606W	30
CAL-11924	03/25/2010	ibc602v9q	F606W	360
CAL-11925	10/20/2009	ibc504v5q	F467M	10
CAL-11925	10/20/2009	ibc504v3q	F467M	500
CAL-11925	10/20/2009	ibc504vdq	F467M	10
CAL-11925	10/20/2009	ibc504veq	F467M	500